**AS ARTS AND SCIENCE**
ARTS AND SCIENCE PRESS PTE. LTD

# Research Article

# Magnetogravimetric study on the Scotia Plate, in the South Atlantic Ocean for the characterization of tsunamis

Arecco M. Alejandra[1,2,*], Larocca Patricia A.[1], Oreiro Fernando A.[3,4], Mora, Mariana C.[3,5], Canero M. Florencia[3]; Fiore Mónica E.[1,2]

[1] *Universidad de Buenos Aires, Facultad de Ingeniería, Instituto de Geodesia y Geofísica Aplicadas.*

[2] *Universidad de la Defensa Nacional, Facultad de la Armada, Escuela de Ciencias del Mar.*

[3] *Ministerio de Defensa, Servicio de Hidrografía Naval, Departamento de Oceanografía.*

[4] *Universidad de Buenos Aires, Facultad de Ingeniería, Departamento de Agrimensura.*

[5] *Universidad Nacional de La Plata, Facultad de Ingeniería, Departamento de Agrimensura.*

**\* Corresponding author:** Arecco M. Alejandra, marecco@fi.uba.ar

## ABSTRACT

The marine and coastal environments of the Scotia Sea regions in the Southern Atlantic Ocean and Antarctica are vulnerable to the potentially disastrous effects from seismic activity in the Scotia Arc. This paper presents a magnetogravimetric study of the Scotia Plate for tsunami characterization. The influence of earthquakes on the Geomagnetic Field (GMF) is investigated using data from INTERMAGNET network observatories. A tectonic model from gravimetric data is evaluated using gravity data from NOAA and seismic refraction data from Lamont-Doherty Earth Observatory oceanic surveys. The study also assesses the impact on water level (WL) measured at 6 tide gauge stations in the region obtained from the Intergovernmental Oceanographic Commission (IOC). The WL records collected are filtered and analyzed to identify tsunamis at each station. Cross Wavelet Transform (XWT) is applied, and a frequency analysis of the GMF is conducted to identify specific frequencies during seismic events. A 2D tectonic model is constructed for the North Scotia Ridge using gravimetric and seismic data to characterize structural boundaries that may be activated during seismic events. The results reveal anomalous frequencies in the GMF horizontal component frequency analysis during the November 25, 2013 earthquake, those results shown great data correlation with [1;1.5] hour periods from different observatories in the study area. Gravimetric modeling delineates faults activated during seismic activity and edges of structures potentially activated due to the margin transcurrent and compressional nature. WL anomalies up to 1.30 m are obtained following earthquakes with a Richter scale magnitude greater than 8 Mw. The tsunami propagation speed in the study area averaged 460 km/h, consistent with the expected speed for those depths, except for Puerto Argentino (PA), which exceeded them by 50%.

*Keywords:* earthquakes; tsunamis; geomagnetic field; 2D gravimetric model; South Atlantic Ocean

## 1. Introduction

The study area is located in the South Atlantic Ocean and is one of the most active seismic regions in the world, especially the Scotia Arc, which includes the Scotia and South Sandwich plates. The Scotia Sea region

is tectonically complex, being composed of other smaller plates: the Scotia and Sandwich Plates. The edges of this active set are represented by various types of margins. (**Figure 1**).

The North Scotia Ridge, which extends from Tierra del Fuego, through the Burdwood/Namuncurá Bank, up to the South Georgia Islands, is mainly represented by a transcurrent and convergent margin. To the east is the Sandwich microplate, separated from the Scotia plate by an active accretionary margin. The Sandwich microplate presents a trench, product of the South American plate subduction beneath the Sandwich microplate (Bohoyo *et al.*, 2007[1]; Dalziel *et al.*, 2013[2]).

The Southern Scotia Plate is represented by a combined transcurrent and accretionary margin. The Scotia Plate is made up of oceanic lithosphere and small continental fragment crust (Yamin and Anselmi, 2020[3]). It can be seen as the link between two major plates, the South American to the north, and the Antarctic to the south and west, its origin being related to the interaction between these plates during the Cenozoic.

The South American plate subduction zone beneath the South Sandwich plate, located in the South Atlantic, represents one of the greatest seismic and volcanic activity areas on the planet. In the 1970 - 2021 period, more than 4,900 seismic events of magnitude greater than 4.5 Mw were detected (Beniest and Schellart, 2020[4]). Therefore, it is one of the regions of the South Atlantic Ocean with great potential for tsunamis generation (Dragani *et al.*, 2009[5]).

The Argentine Atlantic coast vulnerability has been studied by many authors (Pérez *et al.*, 2022[6]; Dato *et al.*, 2020[7]; Dragani *et al.*, 2011[8], 2015[9]). In addition, Patagonian coast tsunami risk, generated by earthquakes located in the Scotia Arc region from numerical and tectonic models were studied by many authors (Dragani *et al.*, 2009[5]; Mora, 2023[10]). The Argentine coasts, Malvinas Islands, South Georgia Islands and Antarctic Bases are frequently subjected to Water Level (WL) rise events, due to meteorological effects, such as meteotsunami and Storm Surge (SS) and by seismic action. Arecco *et al.* (2023)[11] recorded abnormal sea height levels along the Argentine coast and Antarctic bases during the Mw 8.1 earthquake of August 12, 2021 in the Sandwich Islands, recording heights above 1.3 m in the South Georgia Islands.
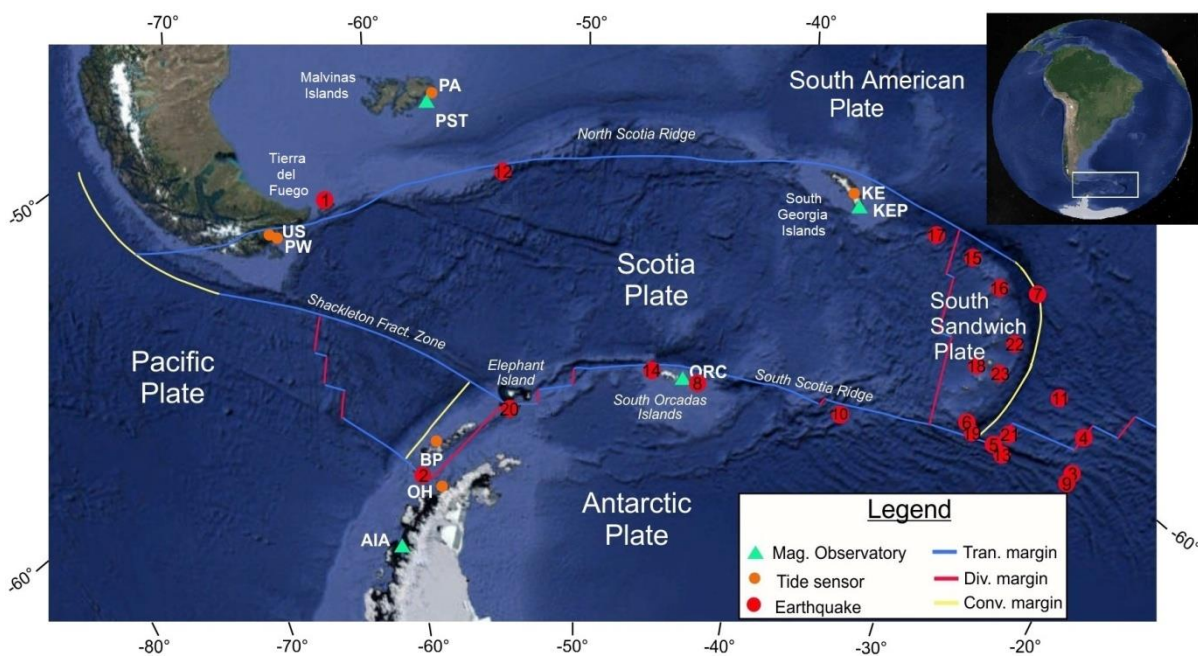


**Figure 1.** Location of Mw ≥ 6.6 earthquakes in the last 20 years around the Scotia Plate. Earth's plate boundaries (blue line: transcurrent edge; red line: divergent edge; and yellow line: convergent edge). Geomagnetic observatories (green triangles): Puerto Argentino (PST), King Edward Point (KEP), Argentine Island - Antarctica (AIA), Orcadas Islands (ORC). Tide stations (orange dots): King Edward (KE), Puerto Argentino (PA), Base Prat (BP), O'Higgins (OH), Puerto Williams (PW), Ushuaia (US).

There are numerous studies reporting associations between earthquakes and physical phenomena, such as electromagnetic field variations (Varotsos *et al.*, 2013[12]; Hayakawa *et al.*, 2010[13]; Takeuchi *et al.*, 2012[14]; Gao *et al.*, 2014[15]; Zhao *et al.*, 2021[16]), anomalous Geomagnetic Field (GMF) records on the earth's surface (Ruiz *et al.*, 2011[17]; Takla *et al.*, 2018[18]; Arecco *et al.*, 2020[19]; Larocca *et al.*, 2021[20])

In addition, historical documents provide us with critical information to infer huge historical earthquakes and tsunamis. Simulation, amplification and propagation studies of underwater earthquakes located in the Scotia Arc from numerical simulations (Dragani *et al.*, 2009)[5].

This work selects earthquakes of magnitude greater than 6.6 occurred between 1970 and 2021 in the study area, and performed frequency analyzes on GMF time series before and after the earthquakes, in order to find relationships within frequencies. Numerical filter is applied to the WL heights post seismic activity enabling the calculation of tsunami heights that affected the coasts of the region. Finally, a gravimetric tectonic model, transverse to the North Scotia Ridge, is developed, and faults in the crust with potential activation during seismic activity are explored.

## 2. Area under study

The Scotia Sea is tectonically complex, being composed of other smaller plates: the Scotia and Sandwich. The plate boundaries around the Scotia Sea to the North and South are of a transcurrent type, known as North Scotia Ridge and South Scotia Ridge, respectively. To the East lies the oceanic ridge that divides the Scotia Plate from the Sandwich Plate, and further East runs the Sandwich del Sur Trench, which is the topographic expression of the oceanic South American Plate subducting below the Sandwich del Sur Islands.

The origin of the Scotia Plate is associated with the Antarctic Peninsula and South American plate separation, hence   its formation by a large surface of oceanic lithosphere, small fragments of continental crust and the development of small ocean basins; as well as the generation of the Scotia ridges and the Sandwich plate.

Its northern and southern edges have sinistral transform movements, represented by the Magallanes-Fagnano fault, the North Scotia Ridge and the South Scotia Ridge respectively. The Chilean trench southern extension is the Shackleton Fracture zone, being the western limit of the Scotia plate with Antarctica.

Pelayo and Wiens suggest that (1989)[21] the North Scotia Ridge has a transpressive boundary, meaning a combination of compression and shearing, due to the presence of an almost continuous line of small continental lithospheric fragments (the Tierra del Fuego block, Burdwood, Davis, and Aurora banks, and the South Georgia block). These fragments exhibit compressional deformation for at least the past 7 Ma (Cunninghan *et al.*, 1998[22]). They propose a left-lateral relative motion of 0.5 cm/year for this boundary and, in an absolute reference frame (Gordon *et al.*, 1988[23]), a Scotia Plate movement toward the WSW at 2.2 cm/year.

## 3. Data

In order to characterize the tsunamis that could affect coastal populations and exposed regions, seismic, WL, GMF and Gravity data were evaluated. The institutions that provide data are: i) seismological data from United States Geological Survey (USGS) available at https://earthquake.usgs.gov/earthquakes/search/, ii) time-series of WL heights from tide stations of the Intergovernmental Oceanographic Commission (IOC) available at https://www.ioc.unesco.org/en, iii) time series of GMF data from observatories of the International Real-time Magnetic Observatory Network (INTERMAGNET) available at https://intermagnet.org/ and iv) to build a tectonic model, gravity anomaly grids from National Center for Environmental Information (NCEI) of United States National Oceanic and Atmospheric Administration (NOAA) available at

3

https://www.ncei.noaa.gov/, global bathymetry grid ETOPO1 (Amante and Eakins, 2009[24]), geologic map from Argentine Mining Geological Service (SEGEMAR) available at https://repositorio.segemar.gov.ar/handle/308849217/66 to obtain geological information, and sedimentary thickness data were applied. In addition, own data from compilations of the sedimentary thickness and depth of the Mohorovičić discontinuity (Arecco *et al.*, 2016)[25] from the *Institute of Geodesy and Applied Geophysics of the University of* Buenos Aires (UBA) were utilized.

### 3.1. Seismic data

The USGS monitors and reports on earthquakes, assesses earthquake impacts and hazards, and conducts targeted research on the causes and effects of earthquakes. These activities are carried out as part of the broader National Earthquake Hazard Reduction Program (NEHRP). Since 1970, in this area there have been more than 20 seismic events of Mw>6.6, of which over a half have exceeded a magnitude of Mw7 (**Table 1**).

From Table 1, five earthquakes were chosen that were (**bold**) representative of each Scotia Arc plate boundary types, that is, the North and South Scotia Ridges and the Sandwich Trench and, in addition, that had concurrent data from GMF and WL.

**Table 1.** Seismic events of Mw > 6.6 from 1970 to 2021. Date, magnitude and location. Information from the USGS. (SSI: South Sandwich Islands).

| N° | Date | Latitude (°) | Longitude (°) | Depth(km) | Magnitude ($M_w$) | Region |
|---|---|---|---|---|---|---|
| 1 | 1970-06-15 11:14:51 | -54.476 | -64.499 | 10 | 7.2 | Tierra del Fuego, Argentine |
| 2 | 1971-02-08 21:04:20 | -63.398 | -61.377 | 12.5 | 7 | South Shetland Islands |
| 3 | 1973-10-06 15:07:37 | -60.823 | -21.549 | 33 | 7 | East of the SSI |
| 4 | 1977-08-26 19:50:01 | -59.426 | -20.508 | 33 | 7.1 | East of the SSI |
| 5 | 1983-10-22 04:21:35 | -60.665 | -25.451 | 24 | 7.2 | SSI |
| 6 | 1987-01-30 22:29:42 | -60.063 | -26.916 | 47.6 | 7 | SSI |
| 7 | 1991-12-27 04:05:58 | -56.032 | -25.266 | 10 | 7.2 | SSI |
| 8 | 2003-08-04 04:37:20 | -60.532 | -43.411 | 10 | 7.6 | Scotia Sea |
| 9 | 2006-01-02 06:10:49 | -60.957 | -21.606 | 13 | 7.4 | East of the SSI |
| 10 | 2006-08-20 03:41:48 | -61.029 | -34.371 | 13 | 7 | Scotia Sea |
| 11 | 2008-06-30 06:17:43 | -58.227 | -22.099 | 8 | 7 | South Sandwich Islands region |
| 12 | 2013-07-15 14:03:39 | -60.857 | -25.07 | 11 | 7.3 | 218 km SSE of Bristol Island, SSI |
| **13** | **2013-11-17 09:04:55** | -60.2738 | -46.4011 | 10 | 7.7 | Scotia Sea |
| **14** | **2013-11-25 06:27:33** | -53.9451 | -55.0033 | 11.8 | 7 | Malvinas zone |
| 15 | 2014-06-29 07:52:50 | -55.4703 | -28.3956 | 8 | 6.9 | 154 km NNW of Visokoi Island |
| 16 | 2016-05-28 09:46:59 | -56.2409 | -26.9353 | 78 | 7.2 | 53 km NNE of Visokoi Island, SSI |
| **17** | **2016-08-19 07:32:22** | -55.2852 | -31.8766 | 10 | 7.4 | South Georgia Island |
| 18 | 2018-12-11 02:26:29 | -58.5446 | -26.3856 | 133 | 7.1 | 54 km N of Bristol Island, SSI |
| 19 | 2019-08-27 23:55:19 | -60.2152 | -26.5801 | 11.8 | 6.6 | 131 km S of Bristol Island, SSI |
| 20 | 2021-01-23 23:36:50 | -61.8117 | -55.4903 | 9.8 | 6.9 | South Shetland Islands |
| **21** | **2021-08-12 18:32:52** | -57.5674 | -25.0131 | 47 | 7.5 | SSI |
| **22** | **2021-08-12 18:35:20** | -58.4513 | -25.327 | 55.7 | 8.1 | SSI |
| 23 | 2021-08-22 21:33:20 | -60.2897 | -24.8801 | 14 | 7.1 | SSI |

## 3.2. Water Level data

The IOC data center provide information about real-time sea-level stations from the global and regional networks operational status, and provide a display service for quick inspection of the raw data stream from individual stations. The IOC offers a map and a list of active tide gauge stations which provide WL information from 2 or more sensors - radar, pressure or atmospheric pressure -. These stations supply information on the relative average level in daily or monthly periods per minute. For this work, the most complete data series at each station was selected. The data was extracted from the tide stations: King Edward (KE) (54.28° S; 36.5° W), Puerto Argentino (PA) (51.75° S; 57.93° W), Base Prat (BP) (62.48° S; 59.66° W), O'Higgins (OH) (63.32° S; 57.90° W), Puerto Williams (PW), (54.93° S; 67.61° W), Ushuaia (US) (54.82° S; 68.22° W), provided by the Sea Level Station Monitoring Facility (https://www.ioc-sealevelmonitoring.org/list.php) (Figure 1). Table 2 shows the stations and the sensor available with selected WL records on the date of the seismic events.

**Table 2.** Stations with selected WL data on the earthquake date, and type of sensor recording the data (Pressure: P; Radar: R).

| Date | Depth(km) | Mag($M_w$) | KE | PA | BP | OH | PW | US |
|------|-----------|-----------|-----|-----|-----|-----|-----|-----|
| 2008-06-30 | 8 | 7 | - | R | - | - | P | - |
| 2013-07-15 | 11 | 7.3 | P | R | P | - | P | - |
| 2013-11-17 | 10 | 7.7 | P | R | P | - | P | - |
| 2013-11-25 | 11.8 | 7 | P | R | P | - | P | - |
| 2016-05-28 | 78 | 7.2 | P | P | P | - | P | R |
| 2016-08-19 | 10 | 7.4 | P | P | P | - | P | R |
| 2018-12-11 | 133 | 7.1 | P | - | P | - | P | R |
| 2021-08-12 | 47 | 7.5 | P | P | P | P | P | R |
| 2021-08-12 | 55.7 | 8.1 | P | P | P | P | P | R |
| 2022-08-12 | 14 | 7.1 | P | P | P | P | P | R |

## 3.3. Geomagnetic field data

The International Network of Real-Time Magnetic Observatories is a global network of observatories that monitor the Earth's magnetic field. On this site you can find data and information from geomagnetic observatories around the world. The GMF data comes from INTERMAGNET network selected observatories in the area. These are King Edward Point (KEP) (54.3° S; 36.5° W), Puerto Argentino/Port Stanley (PST) (51.7° S; 57.8° W), Orcadas Islands (ORC) (60.7° S; 44.7° W) and Faraday Islands Argentine Island-Akademik Vernadsky Base (AIA) (65.25° S; 64.25° W), whose data are available at https://intermagnet.github.io. These observatories provide information about GMF components per minute.

## 3.4. Tectonic model data

Tectonic models are attempts to simulate conceptually, mechanically, or mathematically deformation of the Earth's crust. Since almost no geologic structure can be adequately observed either geometrically or throughout the process of formation, one logical approach is to construct a scale model. These models can be represented in 3D or 2D. The 2D gravimetric inversion model consists of obtaining 2D models of blocks/structures that make up the crust, whose density, depth and shape characteristics satisfy the profiles of the observed gravimetric field.

A gravimetric model requires, in addition to gravity data, extra information that will act as a constraint of the model. The 2D gravimetric model required free-air gravimetric anomaly data for modeling, geological and

seismic information for the arrangement of major tectonic structures, and geophysical information for the densities of the structures. In addition, information on the sea depth and the thickness of the Earth's crust are required.

In this study, free-air anomaly data were obtained from the NCEI, NOAA database, which is available at www.ngdc.noaa.gov/mgg/GEODAS/GEODAS.html. Information regarding model constraints is derived from the refraction seismic geophysical method carried out during oceanographic surveys by Lamont-Doherty Earth Observatory (LDEO) in the United, as published Ewing *et al.* (1971)[26]. Furthermore, these studies provided information on the velocity, and therefore the density of the underlying structures detected.

The Mohorovičić discontinuity depth and the sea sedimentary thickness come from a compilation of specialized geophysics publications, which was conducted at the Institute of Applied Geodesy and Geophysics of the Faculty of Engineering at UBA published by (Arecco *et al.*, 2016)[25].

The 2D gravimetric model relied on seismic section C-D, as described by Ewing *et al.* (1971)[26]; its trace can be seen in Figure 2. This seismic section provides the general arrangement and the subsurface structures location and the Scotia Plate, the North Scotia Ridge, the Davis Bank, the Malvinas Trench, and the Malvinas Plateau average recorded velocities.
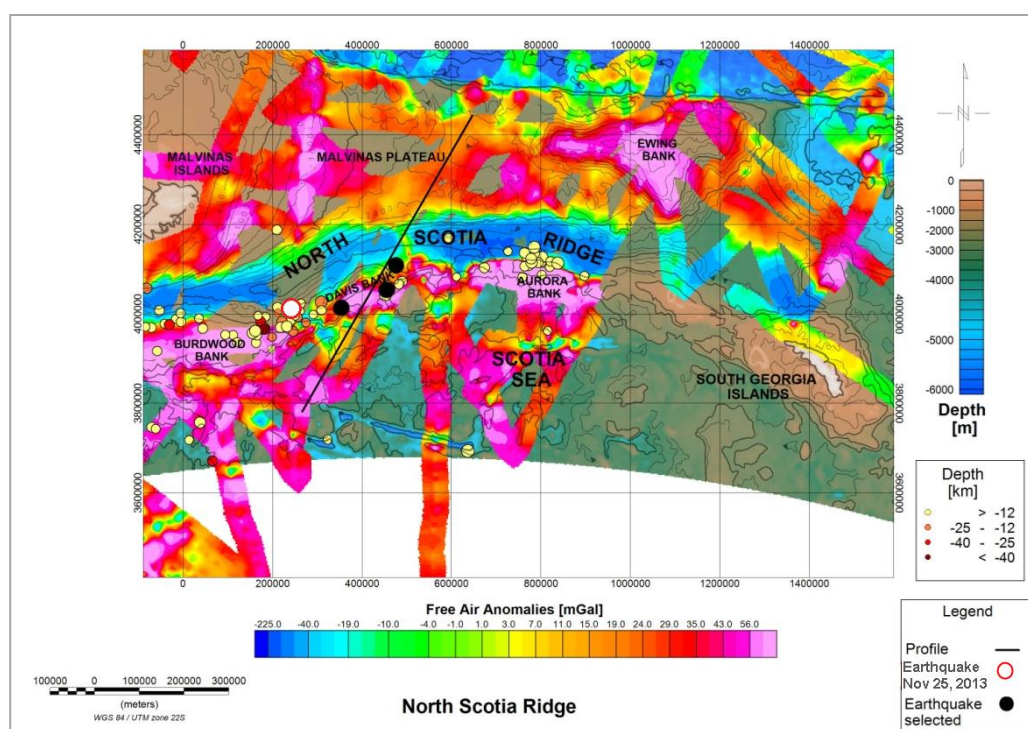


**Figure 2.** Map of FAA (Free Air Anomalies) of the North Scotia Ridge from oceanographic surveys information (NCEI) overlaid on ocean depths from (ETOPO). Depth contours every 200 m (black curves). Trace of the gravimetric model profile (black line). Earthquakes (circles). Selected earthquakes (black circles).

The sea depths were obtained from the global ETOPO1 grid (Amante y Eakins, 2009)[24], provided by NOAA (available at http://www.ngdc.noaa.gov/mgg/global/global.html), and the Mohorovičić discontinuity depth comes from the grid provided by Arecco *et al.* (2016)[25].

## 4. Methodology

Earthquakes in the study region are the source that feeds the analysis carried out on WL and GMF in the search for the characterization of tsunamis and their characteristic frequencies.

WL time series contain a lot of information, such as tide, storm surge, seiches, tsunamis, etc., therefore, they must be filtered to break down the research object. In this case it is necessary to isolate the earthquakes influence (tsunamis) from the WL time series.

This work applies the Wavelet transform to the GMF time series with the purpose of locating both the time and frequency of these non-stationary time series focused on periods of occurrence of the studied earthquakes.

Tectonic modeling by gravimetric inversion allows modeling large structures of the Earth's crust. In particular, in the study area, it is of interest to find faults in those structures of the oceanic crust that, due to the action of earthquakes, are activated, lifting blocks and seawater, thus causing tsunamis.

## 4.1. WL data treatment

WL information from available sensors was downloaded for each event, and their quality was controlled using the methodology applied for the network of tide stations of the Argentine Naval Hydrographic Service according to D'Onofrio (1984) [27]. From the cleaned data, harmonic analysis was performed, following the methodology applied by Oreiro *et al.* (2014) [28], for the sites where harmonic constants were not available (BP, PW, OH and KE). Series with at least two years of observations were used, and constituents with amplitudes greater than 5 mm were selected. For all stations, astronomical tidal predictions were made 1 day before and 4 days after the moment in which each earthquake occurred.

The determination of these harmonic constants allowed a prediction of the height of the tide for each location of the tide gauge stations. From this prediction and in order to obtain the tsunami waves, the tidal predictions were extracted from the records, then obtaining the WL Residues according to (Eq.1).

$$Residues_{WL} = Records_{WL} - Tide \tag{Eq.1}$$

Where $Residues_{WL}$ contains information of tsunami high, $Records_{WL}$ is the refined information from the sensors and *Tide* is the prediction for each tide gauge stations.

## 4.2. Magnetic field data treatment

The classic treatment was applied to the GMF data consisting of removing the IGRF by subtracting the corresponding component. As the time series of geomagnetic data are non-seasonal and linear, it is appropriate to perform the analysis with adequate methods, such as the continuous wavelet transform (CWT) which, within the mathematical field of harmonic analysis, provides an optimum resolution in the time-frequency plane, thus allowing for an excellent characterization of the series (Grinsted *et al.*, 2004)[29].

For this purpose, the CWT was applied to the CMF data from the observatories nearest (KEP, PST and AIA) using the Morlet wavelet (with $\omega_0 = 6$) because it provides an adequate time-frequency balance.

The geomagnetic observatories provide the intensity of the daily GMF components per minute, of which the horizontal component (H) was chosen because it is very susceptible to rapid GMF variations.

The GMF observations contain information about the Earth's main magnetic field, the variations resulting from the effect of solar activity and any other magnetic variations that occur in the observatory area.

In order to highlight local magnetic variations and isolate them from solar activity, the observatories' paired data were selected, considering the earthquake proximity to the observatory network according to Larocca *et al.* (2021)[20]. Therefore, the differences calculated, referred to as deltas (ΔH) minimized the solar diurnal variation effects.

A wavelet is a function with zero mean and that is localized in both frequency ($\delta\omega$ or the bandwidth) and time ($\delta t$). The CWT is to apply the wavelet as a band pass filter to the time series. The wavelet is     stretched in time (t) by varying its scale (s), so that $\eta=s \cdot t$, and normalizing it to have unit energy.

One particular wavelet, for example the Morlet, is defined (Eq.2).

$$\psi_0(\eta) = \pi^{-1/4} e^{i\omega_0\eta} e^{\frac{-\eta^2}{2}} \tag{Eq.2}$$

where $\omega_0$ is dimensionless frequency and $\eta$ is dimensionless time. For the Morlet wavelet (with $\omega_0=6$) the Fourier period ($\lambda=wt$) is almost equal to the scale ($\lambda wt=1.03s$). The CWT of a time series ($x_n, n=1,...,N$) with uniform time steps $\delta t$, is defined as the convolution of xn with the scaled and normalized wavelet (Eq.3).

$$W_n^x(s) = \sqrt{\frac{\delta t}{s}} \sum_{n'=1}^{N} x_{n'} \psi_0\left[(n'-n)\frac{\delta t}{s}\right] \tag{Eq.3}$$

The wavelet power is defined as $|W_n^x(s)|^2$. The complex argument of $W_n^x(s)$ can be interpreted as the local phase.

The cross wavelet transform (XWT) of two time series $x_n$ and $y_n$ is defined as $W^{XY}=W^X W^{Y*}$, where$*$ denotes complex conjugation. The complex argument arg ($W^{xy}$) can be interpreted as the local relative phase between both series in time frequency space (Grinsted *et al.*, 2004)[29].

Cross-correlations are among the simplest and most broadly useful tools in signal processing, providing a quantitative measure of the similarity of two waveforms.

Cross Wavelets Correlation (XWT) was applied on the CWT of the deltas ($\Delta H$) between the AIA-KEP and AIA-PST observatories, with the purpose of characterizing the ranges of anomalous frequencies with the best correlation (clockwise the horizontal black arrows) located before of the occurrence of earthquakes.

### 4.3. Gravity inversion modeling

Gravitational modeling is an interactive process for constructing subsurface structural models based on gravity data, geological information, and constraints imposed by data from other geophysical methods.

The geometric gravity models used to calculate the inversion of gravity anomalies represent structures or source bodies of real anomalies. Despite the method's ambiguity, the imposition of simple constraints on admissible solutions, based on geological knowledge and integration with other independent data, generally leads to robust results (Nabighian *et al.*, 2005)[30].

The algorithms used for this modeling are based on Parker (1974) [31] with improvements by Caratori *et al.* (2007)[32]. Modern modeling methods facilitate the use of an iterative procedure. An initial model is postulated with assumed geometry and density contrast for the anomalous body. The gravity anomaly of the body is then calculated and compared with the residual anomaly. The model parameters - shapes and densities of source body - are modified slightly, typically interactively through a graphical interface, and the calculation is repeated until the discrepancies between the model anomaly and the residual anomaly are acceptable to the user.

The modeled profile goes though part of the Malvinas Plateau and Trench and the North Scotia Ridge until reaching the Scotia Sea, covering a length of 752 km (**Figure 2**).

The constraints of the source body shapes were taken from different sources such as: i) the ETOPO global grid for the water body, ii) the publication by Arecco *et al.* (2016)[25] for sediment bodies, and mantle, and iii)

the publication by Ewing *et al.* (1971)[26] for shallow structures beneath the seafloor and bottom sediments, from marine refraction seismic surveys.

It should be noted that the sediment bodies and shallow structures come from the compilation of marine refraction seismic from local campaigns. And the upper mantle top comes from the calculation by inversion of local gravity and the fixed by seismic refraction and reflection of local oceanographic surveys.

The initial densities adopted for modeling were taken from local studies published by: i) Arecco *et al.* (2016)[25] and Introcaso (2003)[33] for the water body, sediments and upper mantle, and ii) Ewing *et al.* (1971) [26] for shallow structures beneath the seafloor.

The initial densities of model blocks represent mean values following the velocity–density conversion law by Brocher (2005)[34]. Both model block borders and densities were adjusted throughout modeling.

Three shallow earthquakes were added to the information on the blocks and densities for modeling, on November 12, 1992 (5.9Mw), on November 3, 2000 (4.7Mw) and on December 25, 2013 (5Mw) very close to the profile (< 50 km) and of medium magnitudes (**Figure 2**). These facilitated the modeling of faults due to the concept of an earthquake as a cortical rupture.

# 5. Observational results

## 5.1. Fast water level variations post-earthquakes

The results of WL variations following seismic events on November 25, 2013, November 17, 2013, August 19, 2016, and August 12, 2021 are shown in Figures 3, 4, 5, and 6, respectively.

The seismic event on November 17, 2013 (**Figure 3**), produces a disturbance in the WL at KE of approximately 0.40 m, arriving 2.5 hours later. Whereas at the other stations no disturbance is perceived. The distance between the seismic location and the KE station is approximately ~880 km (447 Nautical Miles), so it is estimated that the wave reached a speed of 370 km/h (203 knots). The BP record shows a group of small oscillations of a few centimeters in amplitude arriving 2.5 hours later, traveling 725 km from the south of the Scotia Sea, therefore, the tsunami wave developed 207 km/h (111kn).

The records of this tsunami show 4 wave fronts separated in time approximately 60 minutes in KE. Given the distance and depth from the epicenter to the tide gauge station, we estimate a wavelength of approximately 400 km on average.
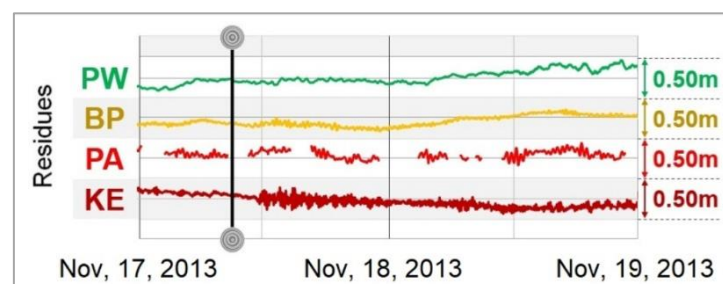


**Figure 3.** Residuals of Water Level (WL) following the earthquake on November 17, 2013, at 9:04 AM (UT). Tide gauge stations: King Edward Point (KE), Puerto Argentino (PA), Base Pratt (BP), and Puerto Williams (PW). Time of the seismic event (black vertical line).

Similarly, in the case of the seismic event on November 25, 2016 (**Figure 4**), there is a disturbance in the WL at KE, but this time only about 0.30 m, arriving 7 hours later. Repeating the wave speed calculation, it traveled ~1200 km (647 Nautical Miles), resulting in a speed of 150 km/h (82 knots). While the tsunami wave reached PW with a speed of 200 km/h (110 kn).

9

The records of this tsunami show 3 wave fronts separated in time approximately 40 minutes in KE. Given the path and depth from the epicenter to the tide gauge station, we estimate a wavelength of approximately 100 km on average.

In the PA record, due to several cuts in the record due to problems with the recording equipment, it is not possible to detect the characteristic oscillations of the tsunami wave that was detected in KE.
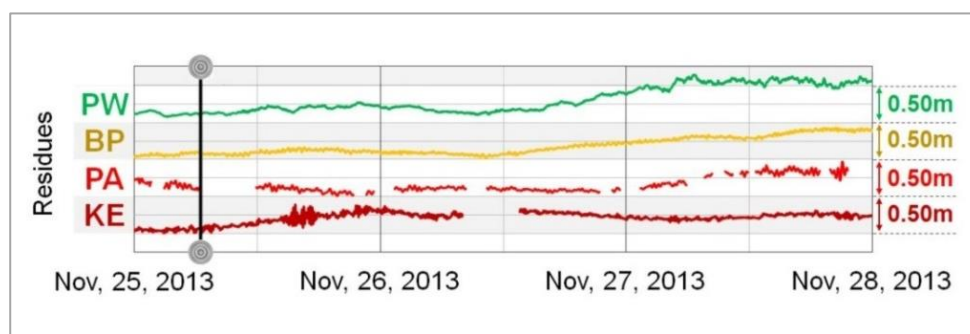


**Figure 4.** Residuals of Water Level (WL) following the earthquake on November 25, 2013, at 6:27 AM (UT). Tide gauge stations: King Edward Point (KE), Puerto Argentino (PA), Base Pratt (BP), and Puerto Williams (PW). Time of the seismic event (black vertical line).

The earthquake on August 19, 2016 (**Figure 5**), produces a WL disturbance only at the KE station, similar to the previous case, of 0.30 m, arriving just under 1 hour after the earthquake. To calculate the wave speed, we estimate a distance between KE and the seismic location of 320 km, so the wave reached a speed of approximately 317 km/h (173 knots). Whereas the tsunami wave reached BP with a speed of 450 km/h (250 knots). The propagation speeds are consistent with the ocean depths that cross the path of the wave and also the height of the wave is lower in shallow areas.
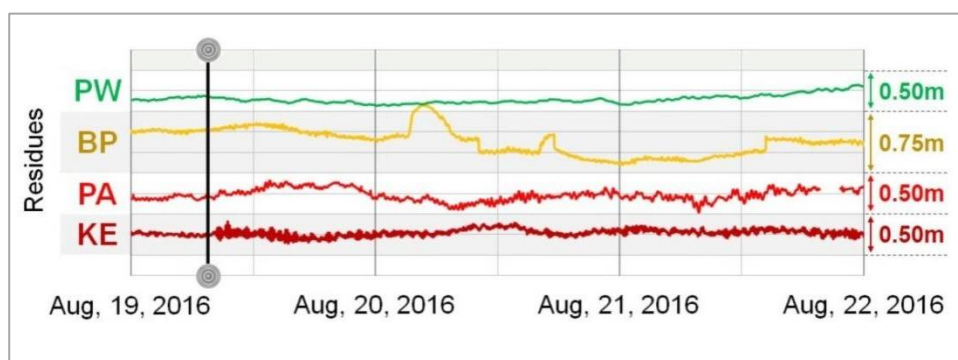


**Figure 5.** Residuals of Water Level (WL) following the earthquake on August 19, 2016, at 7:32 AM (UT). Tide gauge stations: King Edward Point (KE), Puerto Argentino (PA), Base Pratt (BP), and Puerto Williams (PW). Time of the seismic event (black vertical line).

The earthquakes on August 12, 2021 (**Figure 6**), with magnitudes of 7.5 and 8.1 Mw, occurring at 18:32/18:35, cause disturbances at all tide gauge stations in proportion to the distance between the seismic location and the stations. The calculated wave propagation velocities yielded consistent values among themselves (**Table 3**).

The records of this tsunami show 2 wave fronts separated in time approximately 40 min in KE. Given the distance and depth from the epicenter to the tide gauge station, we estimate a wavelength of approximately 300 km on average.

**Table 3.** Wave propagation speeds of the tsunami on August 12, 2021, in the Scotia Sea.

| Station | Time (hours) | Distance (km) | Speed (km/h) | Speed (kn) |
|---------|--------------|---------------|--------------|------------|
| US | 5.5 | 2700 | 491 | 265 |
| PW | 5.5 | 2600 | 473 | 255 |
| OH | 4.25 | 1900 | 447 | 241 |
| BP | 4.55 | 1970 | 433 | 234 |
| PA | 3.65 | 2200 | 603 | 317 |
| KE | 1.75 | 800 | 457 | 247 |
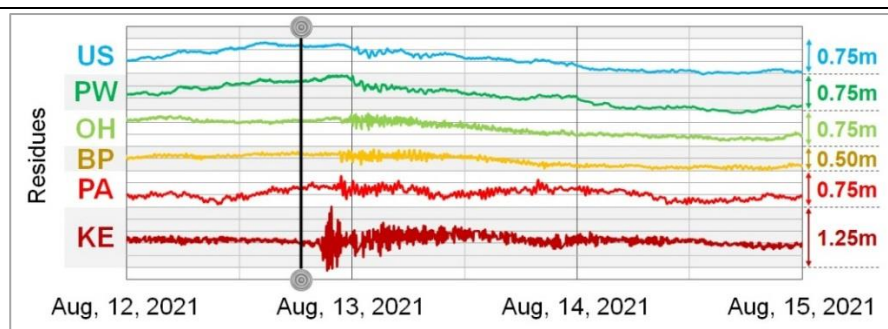


**Figure 6.** Residuals of Water Level (WL) following the earthquake on August 12, 2021, at 18:32 (UT). Tide gauge stations: King Edward (KE), Puerto Argentino (PA), Base Prat (BP), O'Higgins (OH), Puerto Williams (PW), Ushuaia (US). Time of the seismic event (black vertical line).

## 5.2. GMF frequency analysis

The wavelet transform frequency analysis was carried out from November 25, 2013 GMF data, chosen because of the earthquake occurred at 6:27 a.m. (UT) near Malvinas Islands observatory (PST). This occurred at a depth of 11 km with an intensity of 7 Mw, considered a significant earthquake by USGS. The deltas between the horizontal components of the GMF measured in the PST, AIA and KEP observatories were represented: the raw data (**Figure 7A**) and the XWT cross-correlation according to the methodology previously explained in section 4.2 applied to AIA-PST versus PST-KEP deltas (**Figure 7B**).

In a 10-hour interval centered on the time of earthquake occurrence, great instability was observed over a wide range of frequencies. And a high correlation was observed (parallel black arrows) in the interval from 4:30 to 6:00 a.m., an hour and a half before the event. Periods 40 minutes before the production of the earthquakes were found.

## 5.3. 2D Tectonic-gravitational model

In the model, a series of structures consistent with the tectonics of a ridge were defined by plate movements, translational and compression. In particular, two significant high-density dikes (Dike), blocks of continental crust (CC) and oceanic crust (OC), and a series of thrust faults were identified. These thrust faults separate large sedimentary and crustal structures and were likely activated during shallow-depth earthquakes on November 12, 1992 (5.9Mw), November 3, 2000 (4.7 Mw), and December 25, 2013 (5 Mw).

Additionally, the following features were identified: i) beneath the Scotia Plate, a thick upper oceanic crust (UCC) of ~12 km thickness, a very thin and high-density lower oceanic crust (LOC), ii) on the North Scotia Ridge, a series of fractured and thinned continental blocks, likely responding to the compressive and transcurrent accretionary margin's inherent action, and iii) north of the ridge, two continental blocks separated by a large dyke and a significant crustal thinning (**Figure 8**). Furthermore, a very thick lower continental crust (LCC) was identified. The density values of the identified blocks are shown in **Table 4**.
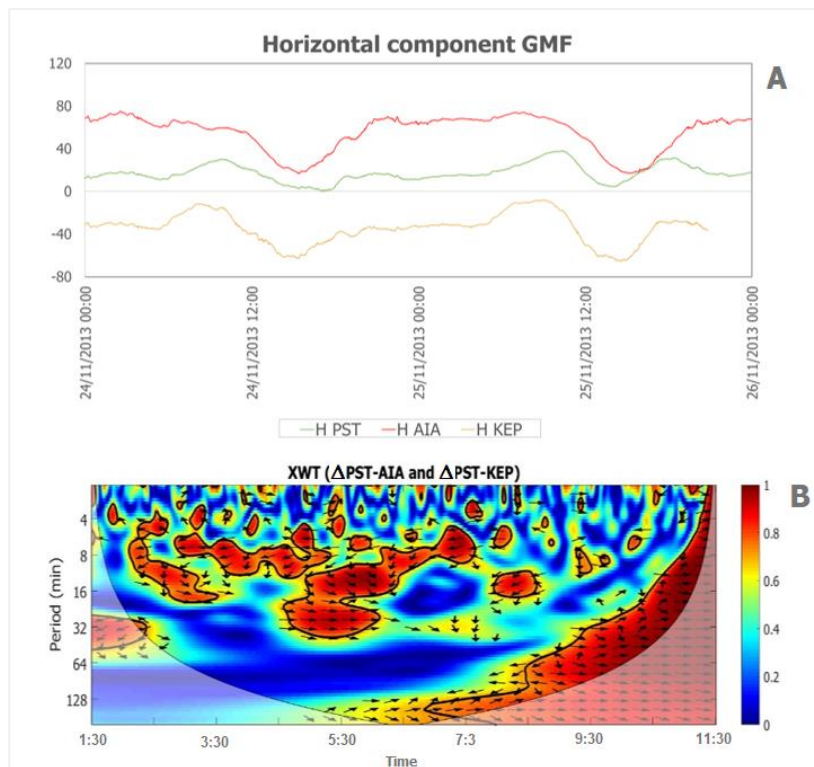
**Figure 7. A.** Horizontal component of the GMF taken at the AIA (red line), PST (green line) and KEP (yellow line) observatories. Data per minute from November 24 to 26, 2013. B. Cross Wavelet Correlation (XWT) during November 25, 2013 event at 6:27 a.m. (UT) [-5;5] hours centered, which occurred in the vicinity of the Malvinas Islands (PST Observatory). The parallel horizontal black arrows, pointing to the right, show areas of direct correlation between the time series. The thick black contour shows a 5% significance level against the red noise background, and the cone of influence (COI) where the edge effects may distort the image is blurred.

In particular, two kinds of block were used to represent the sediments in the Scotia Sea, Davis Bank, Malvinas Trench and Malvinas Plateau, with densities between 2300 and 2350 kg.m$^{-3}$. In the area of the Davis Bank, the blocks are modeled according to Ewing *et al.* (1971)[26].
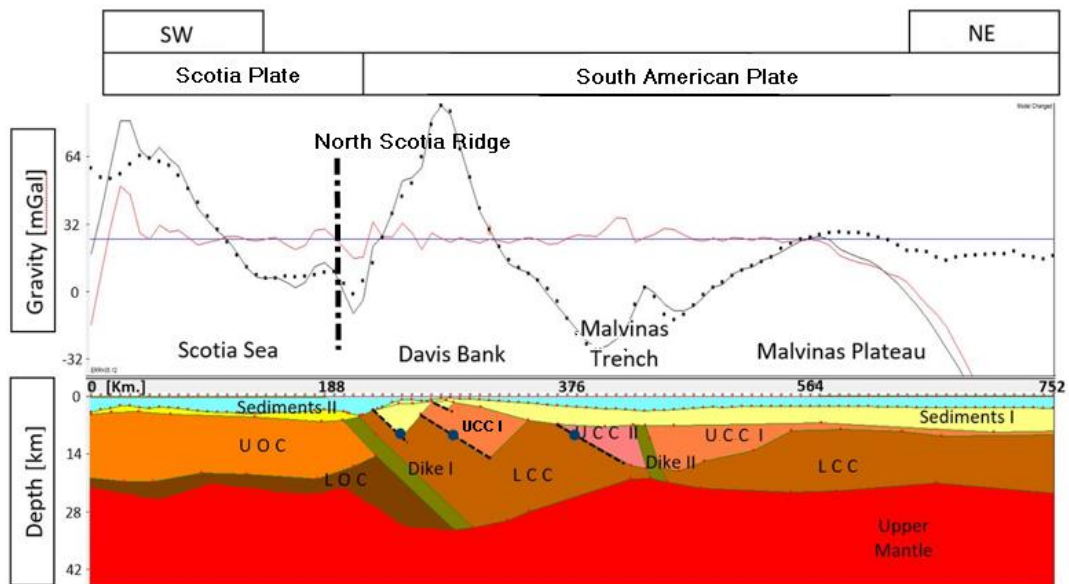


**Figure 8.** Tectonic Model through Free Air Anomaly (FAA) adjustment using the Gravitational Method. Above: Observed FAA (black dots), calculated gravity (black line), and the difference between the calculation and observation (red line). Below, the tectonic subsurface model. References can be found in Table 4. Modeled faults (dashed black lines). Earthquakes (blue dots)

12

**Table 4.** Identified units, corresponding color, and density in accordance with the gravitational tectonic model. Taken from Arecco et al. (2016) [25], Introcaso (2003)[33], Ewing et al. (1971) [26]

| Num. | Structural units | Colour | Density (kg/m³) |
|:---:|:---:|:---:|:---:|
| 1 | Sea water | Cyan | 1026 |
| 2 | Sediments I | Light yellow | 2350 |
| 3 | Sediments II | Dark yellow | 2300 |
| 4 | Dikes | Green | 2950 |
| 5 | Upper Continental Crust I - (UCC I) | Opaque orange | 2670 |
| 6 | Upper Continental Crust II - (UCC II) | Pink | 2600 |
| 7 | Lower Continental Crust   - (LCC) | Light brown | 2780 |
| 8 | Upper Oceanic Crust       - (UOC) | Bright orange | 2790 |
| 9 | Lower Oceanic Crust       - (LOC) | Dark brown | 2900 |
| 10 | Upper Mantle | Red | 3350 |

## 6. Discussion

Our studies on the results of post-earthquake tsunami heights show rapid oscillations in their amplitude and frequency according to Dragani *et al*. (2009)[5]. These rapid oscillations have a duration and frequency similar to the records of the tsunami in Sumatra on December 26, 2004 on the Argentine coasts of Mar del Plata and Santa Teresita, reaching heights of 0.10 to 0.15 m above mean sea level. Other studies show records of WL, between 0.30 m to 1.30 m, in the South Georgia Islands, South Shetland Islands and the Malvinas Islands after earthquakes of magnitude greater than 6.6 Mw in the study area of this work. Furthermore, these studies analyzed the WL and CMF according to the place of origin of the earthquake within the Scotia Arc (Arecco *et al*., 2023) [11].

**Figures 3** and **5** show rapid oscillations over a long period of time approximately 6 to 8 hours, while **Figures 4** and **6** show broader oscillations over a short period of time approximately 1.5 hours followed by a long period of very low amplitude.

The earthquakes studied on the same edge type have similar depth characteristics and show the same response on the GMF components according to Arecco *et al.* (2023)[11] and also show oscillations of different tsunami heights, that is, depending on the margin type.

In relation to the characterization of speed and wavelengths of the tsunamis in this region, the analysis is consistent with the results of Saito and Kubota (2020).

Our speeds propagation studies are consistent with the ocean depths that the wave path traverses and also the height of the wave is lower in shallow areas according to Truong (2012)[36].

All tsunami records were clearly obtained at the KE station, probably because the sensor is located in the open sea unlike the rest that are located in access channels such as PA, US and PW or very sheltered by the destructive dynamic action of the ice, in the cases of Antarctic stations.

The effects of superficial earthquakes in subduction zones over WL usually reach large magnitudes and cause tsunamis of considerable size, such as those that occur in Western Chile or in Japan, where they bring together the 10 most important earthquakes that have been recorded. The group of earthquakes on August 12, 2021, located at 47 and 55 km depth in the South Sandwich Islands trench, generated tsunami records of global expansion that would only be expected for a larger and shallower event. Within the earthquake group Jia *et al.* (2022)[35] showed the existence of a superficial earthquake. The earthquake of November 25, 2013, shows a

record of WL variation as if it had been produced in a subduction zone, so a tectonic-gravimetric profile was studied to identify any structure that may have subducted in the North Ridge of Scotia. This encouraged us to study a tectonic-gravimetric profile in the transcurrent margin, close to the Malvinas Islands, with the purpose of characterizing potentially active faults due to the subduction displacement that occurs in that margin.

In the model a series of structures were defined, which were consistent with the tectonics of a combined continental margin, a combination of a convergent margin and a sheared continental margin of the area (**Figure 8**).

In particular, two structures of significant size are defined: two oblique dykes that accompany the edges of the upper and lower continental crust and a series of faults modeled on three surface earthquakes. Our results are consistent with Urien and Zambrano (1996) [36] who show direct failures in the Davis Bank.

We applied a measure of Cross Correlation Wavelet Transform (XWT) between the two CWTs, to find significant coherence, if the two series are physically related, we would expect a consistent or slowly varying phase. Monte Carlo methods are used to calculate the statistical significance against red noise backgrounds. Cross Correlation Wavelet Transform (XWT) showed in **Figure 7** clearly common features in the wavelet power of the two series such as the significant correlation in the ~1.5 h before the seismic event. From the above analysis, it can conclude that wavelets provide a new tool for the comparison of the periods of earthquakes activity and geomagnetic activity. It could be a possible qualitative mechanism caused by geomagnetic activity that would influence seismic activity: pressure balance of tectonic plates would be interrupted and tension accumulation is enough to trigger seismic activity.

# 7. Conclusions

A series of tsunamis that occurred in the study area were characterized based on a gravimetric model and a geomagnetic study according to the plate boundary of generation of the earthquake.

From the analysis of the Water Level residuals, it is inferred that the shape and length of the oscillations respond to the type of genesis of the earthquake.

The earthquake that occurred on August 12, 2021 (8.1 Mw), in KE the amplitudes of the residuals reached 1.30 m.

Although it did not represent a potential risk, even when combined with storm surge events, and given its significant magnitude, it can be considered as a first indicator of the expected amplitude on the nearby coasts of the region. On the other hand, the propagation speed in the study area, averaged 460 km/h, which is consistent with the speed expected for those depths (approximately 3500 m) except in PA (600 km/h). There are no direct causes that could justify this discrepancy, so the fundaments will be analyzed in subsequent studies.

Potential magnetic precursors could be identified for seismic events in the area of greatest seismic and volcanic activity on the planet. The study of time correlation among seismic events, on November 25, 2013 using an independent method based on the Cross Wavelet Transform (XWT) showed that, high coherence around the corresponding 1.5-to-0.5-hour band, which increases over a period near the occurrence of a seismic event.

The 2D gravimetric tectonic model identified structural blocks consistent with isostatic balance and structural faults. These latest are possibly associated with past seismic events, which can potentially be active due to the release of energy in upcoming events.

The most significant contribution of this tectonic-gravimetric modeling is to complete crustal information that could not be detected by the means used in the background.

## Acknowledgements

## Conflict of interest

The authors declare no conflict of interest.

## References

1. Bohoyo F, Galindo-Zaldívar J, Jabaloy A, et al. Extensional deformation and development of deep basins associated with the sinistral transcurrent fault zone of the Scotia-Antarctic plate boundary, in Tectonics of strike-slip restraining and releasing bends, D. Cunningham (editor), and P. Mann, Special Volume of the Geological Society of London 2007.
2. Dalziel IWD, Lawver LA, Norton IO, et al. The Scotia Arc: Genesis, Evolution, Global Significance. Annual Review of Earth and Planetary Sciences 2013; 41: 767–793. https://doi.org/10.1146/annurev-earth-050212-124155
3. Yamin MG, Anselmi G. Geología de las placas Scotia y Sandwich, revisión y mapa geológico (Spanish) [Geology of the Scotia and Sandwich plates, review and geological map]. SEGEMAR. Serie de Contribuciones Técnicas, Geología Núm. 8. Instituto de Geología y Recursos Minerales 2020.
4. Beniest A, Schellart WP. A geological map of the Scotia Sea area constrained by bathymetry, geological data, geophysical data and seismic tomography models from the deep mantle, Earth-Science Reviews 2020; Volume 210, 103391. https://doi.org/10.1016/j.earscirev.2020.103391.
5. Dragani WC, D'Onofrio EE, Grismeyer W, et al. Vulnerability of the Atlantic Patagonian coast to tsunamis generated by submarine earthquakes located in the Scotia Arc region. Some numerical experiments. Natural hazards 2009; 49(3), 437-458. https://doi.org/10.1007/s11069-008-9289-4.
6. Pérez I, Dragani W, Oreiro F, et al. Meteotsunamis at the Río de la Plata estuary, Estuarine, Coastal and Shelf Science 2022; 277, Article ID 108064. https://doi.org/10.1016/j.ecss.2022.108064.
7. Dato J, Fiore ME, D´Onofrio E, et al. Comparison of the Extreme Surge Estimation with the Generalized Extreme Value Distribution, Using the Maximum of Positive Storm Surge and skew Surge in two port areas with different hydrodynamic and tidal characteristics, J. of Marine Env. Eng. 2020; Vol 00, pp. 1-10
8. Dragani W, D'Onofrio E, Mediavilla D, et al. The Tsunami Threat - Research and Technology. London, IntechOpen. Morner NA (editor), Tide Gauge Observations of the Indian Ocean Tsunami December 26, 2004, at the Rio de La Plata Estuary, Argentina; 2011, p. 355-369. https://doi.org/10.5772/14652.
9. Dragani WC, D'Onofrio EE, Oreiro F, et al. Meteorological Tsunamis: The US East Coast and Other Coastal Regions. New York City, Springer Cham. Vilibic I, Monserrat S, Rabinovich AB (editors). Simultaneous meteorological tsunamis and storm surges at Buenos Aires coast, southeastern South America; 2015, p. 269-280.
10. Mora MC, Arecco MA, Larocca PA. Aplicación de un SIG junto a un programa de modelado 2D al SE de las Malvinas que caracterizan nuevas fallas para prevención de riesgos de tsunamis (Spanish) [GIS Application with a 2D modeling program to the SE of the Malvinas, that characterize new faults for tsunami risk prevention]. 21th LACCEI International Multi-Conference for Engineering, Education and Technology; 2022; Bogota. Fundacion LACCEI   Larrondo Petrie MM , Texier J, Hybrid (editors), 19-21 July 2023. http://dx.doi.org/10.18687/LACCEI2023.1.1.1560

11. Arecco MA, Larocca PA, Oreiro FA, et al. Disturbances in the Geomagnetic Field, Water Level and Atmospheric Pressure associated with Mw> 6.6 earthquakes in the South Atlantic Ocean; Revista Geofísica Internacional 2023. doi.org/10.22201/igeof.2954436xe.2023.62.3.1440

12. Varotsos PA, Sarlis NV, Skordas ES, et al. Seismic Electric Signals: An additional fact showing their physical interconnection with seismicity, Tectonophysics 2013; 589: 116-125. https://doi.org/10.1016/j.tecto.2012.12.020.

13. Hayakawa M, Kasahara Y, Nakamura T, et al. A statistical study on the correlation between lower ionospheric perturbations as seen by subionospheric VLF/LF propagation and earthquakes. Journal of Geophysical Research 2010; 115, A9. https://doi.org/10.1029/2009JA015143.

14. Takeuchi A, Okubo K, Takeuchi N. Electric Signals on and under the Ground Surface Induced by Seismic Waves. International Journal of Geophysics 2012; Article ID 270809, 10 pages. https://doi:10.1155/2012/270809

15. Gao Y, Chen X, Hu H, et al. Induced electromagnetic field by seismic waves in Earth's magnetic field. JGR Solid Earth 2014; 119, 5651–5685. https://doi:10.1002/2014JB010962

16. Zhao J, Gao Y, Tang J, et al. Electromagnetic field generated by an earthquake source due to motional induction in 3D stratified media, and application to 2008 Mw 6.1 Qingchuan earthquake. JGR Solid Earth 2021; 126. https://doi.org/10.1029/2021JB022102.

17. Ruiz F, Sánchez M, Martínez P, et al. La estación magnética Zonda: estudio de perturbaciones magnéticas relacionadas con terremotos. San Juan, Argentina (Spanish) [The Zonda magnetic station: study of magnetic disturbances related to earthquakes. San Juan, Argentina]. 2nd Biennial Meeting of Latinmag 2011; Special Issue. Sinito AM(editor). Latinmag Letters, Vol. 1, Special Issue, A16, 1-7. https://www.geofisica.unam.mx/LatinmagLetters/LL11-0102P/A/A16-Ruiz-corregido.pdf.

18. Takla E, Khashaba A, Abdel Zaher M, et al. Anomalous ultra-low frequency signals possibly linked with seismic activities in Sumatra, Indonesia. NRIAG Journal of Astronomy and Geophysics 2018; 7:2, 247-252. https://doi: 10.1016/j.nrjag.2018.04.004.

19. Arecco MA, Larocca PA, Mora MC. Geomagnetismo y su relación con sismos un estudio, en la micro en la Placa de Sándwich del Sur (Spanish) [Geomagnetism and its relationship with earthquakes, a study, in the micro in the South Sandwich Plate]. Revista Defensa Nacional 2020; N°4, 263-281. https://www.undef.edu.ar/wp-content/uploads/2020/10/04_REVISTA-DEFENSA-NACIONAL.pdf

20. Larocca PA, Arecco MA, Mora MC. Wavelet-based Characterization of Seismicity and Geomagnetic Disturbances in the Sandwich del Sur Microplate Area. Geofísica Internacional 2021; 60, N°4, 320-332. http://revistagi.geofisica.unam.mx/index.php/RGI/article/view/2119/1882

21. Pelayo AM, Wiens DA. Seismotectonics and relative plate motions in the Scotia Sea region. Journal of Geophysical Research 1989; 94: 7293-7320.

22. Cunninghan AP, Barker PF, Tomlinson JS. Tectonics and sedimentary environment of the North Scotia Ridge region revealed by side-scan sonar. Journal of Geological Society, 1998; 941–956. https://doi.org/10.1144/gsjgs.155.6.0941

23. Gordon RG, DeMets C, Argus DF, et al. Current Plate Motions, Eos D'ansactions. American Geophysical Union 1988; 69, 1416.

24. Amante C, Eakins BW. ETOPO1, 1 Arc-Minute Global Relief Model Procedures, Data Sources and Analysis. NOAA Technical Memorandum NESDIS NGDC 2009; 24. https://www.ngdc.noaa.gov/mgg/global/relief/ETOPO1/docs/ETOPO1.pdf.

25. Arecco MA, Ruiz F, Pizarro G, et al. Gravimetric determination of the continental–oceanic boundary of the Argentine continental margin (from 36°S to 50°S). Geophysical Journal International 2016; 204, pp. 366-385. https://doi: 10.1093/gji/ggv433.

26. Ewing JL, Ludwig WJ, Ewing M, et al.  Structure of the Scotia Sea and Falkland Plateau. Journal of Geophysical Research 1971; 76 (29), 7118-7137.

27. D'Onofrio EE. Desarrollo de un nuevo sistema de procesamiento de información de marea. (Spanish) [Development of a new tidal information processing system]. Informe Técnico Nº 25/84. Departamento Oceanografía del Servicio de Hidrografía Naval 1984; 167 p.

28. Oreiro FA, D'Onofrio E, Grismeyer W, et al. Comparison of tide model outputs for the northern region of the Antarctic Peninsula using satellite altimeters and tide gauge data. Polar Science 2014; 8(1), 10-23. https://doi.org/10.1016/j.polar.2013.12.001.

29. Grinsted A, Moore JC, Jevrejeva S. Application of the cross wavelet transform and wavelet coherence to geophysical time series. Nonlin. Process. Geophys 2004; 11, 561-566. https://hal.science/hal-00302394/document

30. Nabighian MN, et al. The Historical Development of the Magnetic Method in Exploration. Geophysics 2005; 70, 33-61. https://doi.org/10.1190/1.2133784.

31. Parker RL. A new method for modeling marine gravity and magnetic anomalies. J Geophys Res 1974; 79, 14, 2014-2016.  https://doi.org/10.1029/JB079i014p02014.

32. Caratori Tontini F, Graziano F, Cocchi L, et al. Determining the optimal Bouguer density for a gravity data-set: implications for the isostatic setting of the Mediterranean Sea, Geophysical Journal International 2007; 169, 380-388. https://doi.org/10.1111/j.1365-246X.2007.03340.x.

33. Introcaso, A. Significativa descompensación isostática en la Cuenca del Colorado (República Argentina), Revista de la Asociación Geológica Argentina 2003; 58, 474–478. http://www.scielo.org.ar/scielo.php?script=sci_abstract&pid=S0004-48222003000300015.

34. Brocher, T.M. Empirical relations between elastic wavespeeds and density in the Earth's crust, Bull. seism. Soc. Am. 2005; 95, 2081–2092. https://pubs.geoscienceworld.org/ssa/bssa/article-abstract/95/6/2081/146858/Empirical-Relations-between-Elastic-Wavespeeds-and?redirectedFrom=fulltext.

35. Jia, Z., Zhan, Z. and Kanamori, H., (2022). Earthquake: A Slow Event Sandwiched Between Regular Ruptures, Geophysical Research Letters, 49, (3). https://doi.org/10.1029/2021GL097104.

36. Truong, H. V. P. Wave-propagation velocity, tsunami speed, amplitudes, dynamic water-attenuation factors. En Proceedings of World Conference on Earthquake Engineering (Red Hook, NY: Curran Associates, Inc.). 2012. p. 1-10. https://www.iitk.ac.in/nicee/wcee/article/WCEE2012_0335.pdf

37. Saito, T. and Kubota T. Tsunami modeling for the deep sea and inside focal areas. Annual Review of Earth and Planetary Sciences, 2020, vol. 48, p. 121-145. https://doi.org/10.1146/annurev-earth-071719-054845